

Article

# Fault Identification of Broken Rotor Bars in Induction Motors Using an Improved Cyclic Modulation Spectral Analysis

Zuolu Wang <sup>1</sup>, Jie Yang <sup>1</sup>, Haiyang Li <sup>2</sup>, Dong Zhen <sup>1,\*</sup> , Yuandong Xu <sup>2</sup>  and Fengshou Gu <sup>2</sup> 

<sup>1</sup> Tianjin Key Laboratory of Power Transmission and Safety Technology for New Energy Vehicles, School of Mechanical Engineering, Hebei University of Technology, Tianjin 300401, China

<sup>2</sup> Centre for Efficiency and Performance Engineering, University of Huddersfield, Huddersfield HD1 3DH, UK

\* Correspondence: d.zhen@hebut.edu.cn

Received: 28 June 2019; Accepted: 21 August 2019; Published: 26 August 2019



**Abstract:** Induction motors (IMs) play an essential role in the field of various industrial applications. Long-time service and tough working situations make IMs become prone to a broken rotor bar (BRB) that is one of the major causes of IMs faults. Hence, the continuous condition monitoring of BRB faults demands a computationally efficient and accurate signal diagnosis technique. The advantage of high reliability and wide applicability in condition monitoring and fault diagnosis based on vibration signature analysis results in an improved cyclic modulation spectrum (CMS), which is one of the cyclic spectral analysis algorithms. CMS is proposed in this paper for the detection and identification of BRB faults in IMs at a steady-state operation based on a vibration signature analysis. The application of CMS is based on the short-time Fourier transform (STFT) and the improved CMS approach is attributed to the optimization of STFT. The optimal window is selected to improve the accuracy for identifying the BRB fault types and severities. The appropriate window length and step size are optimized based on the selected window function to receive a better calculation benefit through simulation and experimental analysis. Compared to other estimators, the improved CMS method provides better fault detectability results by analyzing vertical vibration signatures of a healthy motor, and damaged motors with 1 BRB and 2 BRBs under 0%, 20%, 40%, 60%, and 80% load conditions. Both synthetic and experimental investigations demonstrate the proposed methodology can significantly reduce computational costs and identify the BRB fault types and severities effectively.

**Keywords:** induction motors; broken rotor bar; vibration signature; cyclic spectral analysis

## 1. Introduction

Induction motors (IMs) are considered as the most popular motors in electromechanical energy conversion and various industrial applications. However, various failures in IMs are frequently caused by the operations in harsh environments, continuous wearing, overloads, and unexpected incidents. The broken rotor bar (BRB) fault is one of the most serious failures and needs to be detected on account of its destructiveness. According to the statistics by the Institute of Electrical and Electronics Engineers (IEEE), approximately 9% of IMs faults are due to the BRB, and 8% are caused by BRB faults according to the statistics from the Electric Power Research Institute (EPRI) [1]. If the BRB fault is left undetected and not resolved in time, it can lead to the occurrence of serious BRB faults or other types of motor faults and can waste the electric power. Consequently, the entire motor may collapse, which can result in higher maintenance costs, lower power transmission efficiency, and even serious accidents.

Currently, researchers have applied considerable efforts to the development of effective IMs fault diagnosis technologies for improving operational reliability and reducing downtime. The most widely

applied techniques for BRB faults detection are the motor current signature analysis (MCSA) and the motor vibration signature analysis (MVSA) [2]. Further, magnetic flux measurements have been used, but a flux sensor needs to be installed that can increase the detection costs. Regarding the diagnosis of BRB faults in IMs, a vibration signature analysis can receive satisfactory detection results as well as the MCSA [3]. In addition, the vibration diagnosis is a more reliable and standardized analysis since the measured vibration signals from machines contain useful information reflecting the health conditions of machinery systems. The vibration signature analysis is the most widely used technique in condition monitoring and fault diagnosis due to its simplicity, less comparative cost, and relative ease of the application. Further, no structural changes are required for the application of the vibration analysis for the existing machines [4].

There are a variety of fault diagnosis methods that have been developed based on vibration signal analysis for detecting the BRB faults of IMs. In [5], the advanced use of wavelet analysis by analyzing an axial vibration signal was introduced for BRB faults detection through removing the effects of the interference frequency components. In [6], the Zhao-Atlas-Marks (ZAM) distribution was investigated for BRB faults diagnosis based on vibration transient signals. In a recent work, Rangel-Magdaleno [7] developed a demodulation methodology using discrete wavelet transform (DWT) and autocorrelation methods for the incipient broken bar detection based on MVSA. Delgado-Arredondo [8] presented the complete ensemble empirical mode decomposition (CEEMD) for BRB faults diagnosis, which solves the drawbacks of empirical mode decomposition (EMD) and the ensemble empirical mode decomposition (EEMD) for obtaining accurate analysis results. The orthogonal matching pursuit algorithm (OMP) in [9] focused on the decomposition of signals, which demonstrated the detection method is effective. On the other hand, several MCSA-based demodulation techniques such as empirical mode decomposition (EMD) and neural networks [10], Hilbert-Huang transform (HHT) [11], multiple signal classification (MUSIC) [12], and synchrosqueezing transform (SST) [13] were also developed for BRB fault diagnosis. There are also other techniques such as magnetic field analysis [14], infrared data analysis [15], and air-gap torque analysis [16] that were applied for BRB faults detection.

Despite being powerful signal processing tools and potential applications for BRB fault detection, these diagnosis methodologies mentioned above still have serious shortcomings. They contain substantial computational costs for the exhibition of BRB fault features and lower accuracy for the identification of BRB fault types and severities. For example, solving the intrinsic mode function (IMF) of a signal by using the CEEMD algorithm in [8] is indeed a complicated calculation process. Similarly, the popular methods based on DWT, EMD, HHT, SST, etc., are also faced with low processing efficiency. The estimated parameters used in [7,12] cannot present a clear classification of the BRB fault severities. However, the conventional methods based on a fast Fourier transform (FFT) show its inability to process non-linear and non-stationary vibration signals. Hence, there is an urgent need to develop an accurate and efficient approach for BRB fault diagnosis in IMs.

Furthermore, IMs are typical rotary machines, so that the measured vibration signal from the motor surface has strong periodic modulation characteristics, and these periodically-modulated vibration signals can be regarded as the second-order cyclostationary (CS2) signals. The CS2 signal is the advancement of the first-order cyclostationary (CS1) signal characterized by the mean or expected value, and both CS2 and CS1 signals belong to the category of cyclostationarity [17]. Cyclostationarity refers to a promising signal processing method that has been subverting the field of mechanical signature analysis in recent decades. The conventional Fourier transform (FT) has been proven to be effective in dealing with CS1 components, but it fails to describe CS2 signals because the CS2 signals are complexly modulated. In order to remedy this deficiency, a cyclic spectral analysis was proposed in the 1990s by Gardner and applied to the analysis of CS2 signals [18]. It effectively reconstructs the CS2 signals from a new perspective and extracts the useful information related to mechanical failures. Briefly stated, a cyclic spectral analysis represents the CS2 contents by two frequency variables: Spectral frequency ( $f$ ) and cyclic frequency ( $\alpha$ ). The spectral frequency is employed to exhibit the carrier frequency contents of the signal, and the cyclic frequency aims to indicate the modulation components

leading to the faults [19]. Cyclic spectral analysis is therefore effective in processing non-stationary and non-linear signals, which can reveal the periodic behaviour associated to mechanical faults hidden in the CS2 signals.

According to the advantages of vibration-based fault diagnosis in terms of the cyclic spectral analysis, an improved cyclic spectral analysis method based on the vibration signature analysis was investigated to detect the BRB faults of IMs. One of the cyclic spectral analysis approaches, cyclic modulation spectrum (CMS), that has been described in [20] is referred to and improved on in this paper. The CMS algorithm contains the calculation of the short-time Fourier transform (STFT) method, and it can fully present its value in the diagnosis and identification of a specific mechanical fault by optimizing the use of the STFT. The focus of the present work is to improve the CMS algorithm to get higher accuracy in the classification of BRB fault types and severities and larger computational gains by optimizing the window function, window length and step size for the application of the STFT. Firstly, an optimal window function used in the STFT was selected according to the specific signal form, which can increase the accuracy of identifying the BRB fault types and the severities. Subsequently, the window length and step size were optimized based on the selected window function, which can receive a better computational gain. According to the analysis results in [21], the amplitude of characteristic frequency can be considered as the indicator for the identification of BRB faults. In this paper, the amplitudes of BRB fault characteristic frequencies serve as a criterion for judging BRB fault types and severities. The effectiveness and performance of the proposed method is validated through processing the vertical vibration signals issued from healthy motor and damaged motors with 1 BRB and 2 BRB faults under 0%, 20%, 40%, 60%, and 80% load conditions. Compared to the power spectral density (PSD) [2,3,5,22–25] that has been widely explored for BRB fault detection and other cyclic spectral analysis estimators, such as the cyclic power spectrum (CPS) [26], averaged cyclic periodogram (ACP) [27], and fast spectral correlation (FSC) [28], the improved CMS can provide better diagnosis capability.

This paper is organized as follows: Section 2 briefly presents the information in connection with BRB faults which need to be analyzed and reviews the brief principle of the CMS algorithm. Section 3 introduces the procedures of the improved CMS method. The performance of the improved CMS algorithm for BRB fault feature extraction is validated by simulation studies in Section 4. Section 5 provides the introduction of test rigs and the experimental verification. The conclusions are finally drawn in Section 6.

## 2. Basic Theory of Methodology

### 2.1. BRB Fault Characteristics

The IMs are liable to BRB faults due to both the changing electromagnetic and the mechanical forces. In healthy IMs, the rotor generates symmetrical currents that cause a forward rotating magnetic field at a synchronous speed. If the rotor bar is cracked, a resultant background rotating field can occur [8]. Consequently, the inverse frequency component of the rotor currents at  $-sf_0$  (where  $s$  denotes the slip and  $f_0$  denotes the supply frequency) appears. The inverse sequence components act on the stator side and lead to the frequency components of  $(1 - 2ks)f_0$  (where  $k = 1, 2, 3, \dots$  is any positive integer), and the produced additional frequency information mainly leads to the presence of BRB fault frequency components at  $(f_r \pm 2ksf_0)$  in radial and axial vibration signals [2]. As a result, a torque ripple and a speed oscillation are generated at the frequency of  $2ksf_0$ , which acts as a frequency component modulated on the rotation frequency  $f_r$  in the vibration spectrum that are given by:

$$f_{BRB} = f_r \pm 2ksf_0 \quad (1)$$

where  $f_{BRB}$  is the sideband frequency related to the BRB fault. The slip  $s$  is defined by the mechanical speed ( $n_m$ ) of the IM and the synchronous speed ( $n_s$ ) as expressed [28]:

$$s = \frac{n_s - n_m}{n_s} \quad (2)$$

Further, the research shows  $2sf_0$  is the main modulation component in the BRB fault vibration signals, which helps in identifying BRB faults easily and effectively [29]. In the following analysis,  $2sf_0$  is explored and used as the most important fault feature for BRB faults detection.

## 2.2. Cyclic Modulation Spectrum (CMS)

A cyclostationary signal is a special type of non-stationary signal, and it contains hidden periodicity in the signals associated to mechanical faults. The cyclostationarity covers rich statistical characteristics, thus the cyclostationary signal can be divided into a first-order (mean value) cyclostationary signal, a second-order (correlation function and spectral correlation density) cyclostationary signal, and even a higher-order cyclostationary signal [17]. For cyclostationary discrete signals  $x[n]$  with a length of samples  $L$  and a sampling frequency of  $F_s$ , its time-varying autocorrelation function can be expressed as:

$$R_x[n, \tau] = E\{x[n + \beta\tau]x[n - \bar{\beta}\tau]^*\} \quad (3)$$

where  $\beta + \bar{\beta} = 1$ ,  $n, \beta, \bar{\beta} \geq 0$ ,  $\tau$  represents the time-lag variable, and  $n = 0, 1, \dots, L - 1$ . However, the traditional cyclic spectral correlation analysis methods based on the instantaneous autocorrelation function require high computational costs. In order to improve the efficiency of the calculation, an effective calculation technique, cyclic modulation spectrum (CMS), was proposed by Antoni [20]. This approach contains the calculation of STFT. The STFT of signal  $x[n]$  mentioned above is defined as:

$$X_{STFT} = (k, f_i) = \sum_{n=0}^{Nw-1} x[kR + n]w[n]e^{-j2\pi n \frac{f_i}{F_s}} \quad (4)$$

where the discrete frequency  $f_i = i\Delta f$ ,  $i = 0, 1, \dots, Nw - 1$ ,  $w[n]$  is a data-window of signal  $x[n]$  with  $Nw$ -long data,  $R$  stands for the time shift, the total shift number is  $K$ ,  $K = \lfloor (L - Nw)/R \rfloor + 1$  ( $\lfloor \cdot \rfloor$  represents the largest integer not greater than  $K$ ), and  $k = 1, 2, \dots, K$ . The CMS can be obtained by efficiently calculating the discrete Fourier transform (DFT) of the STFT spectrum. Hence, the CMS of the signal with a data-window based on STFT can be expressed as:

$$S_{CMS}(\alpha, f) = \frac{1}{K\|w\|_2 F_s} \sum_{k=0}^{K-1} |X_{STFT}(k, f)|^2 e^{-j2\pi(kR+M)\frac{\alpha}{F_s}} \quad (5)$$

$$\|w\|^2 = \sum_{n=0}^{Nw-1} |w[n]|^2 \quad (6)$$

where  $M$  denotes the intermediate time value of the window function  $w[n]$  and  $w[M - n] = w[M + n]$ .  $\alpha$  is the cyclic or modulation frequency and  $f$  is the spectral or carrier frequency. The CMS considers the periodic energy of signal in a frequency band of  $\Delta f$ .

$$\Delta f = \frac{F_s}{Nw} \quad (7)$$

Table 1 presents the cyclic frequency resolution  $\Delta\alpha$  and the maximum cycle frequency  $\alpha_{max}$  of four cyclic spectral analysis algorithms and it is noted that they have the advantage of higher cyclic frequency resolution. Although the CMS method can reduce the calculation cost, this approach still has the shortcoming of a limit modulation frequency analysis [28]. Its maximum cyclic analysis frequency is limited to the range of carrier frequency resolution. For example, if the carrier frequency resolution  $\Delta f = 10$  Hz, then the maximum cyclic frequency  $\alpha_{max}$  that can be detected is smaller than or equal to  $\Delta f$ . Therefore, the CMS method can only provide effective analysis results when the carrier frequency resolution can guarantee the analyzable maximum cyclic frequency range meets the needs of the fault diagnosis.

**Table 1.** Cyclic frequency parameters of four cyclic spectral analysis algorithms.

Cyclic Frequency	CPS	ACP	CMS	FSC
$\Delta\alpha$	$F_s/L$	$F_s/L$	$F_s/L$	$F_s/L$
$\alpha_{max}$	$F_s/2$	$F_s/2R$	$F_s/Nw$	$F_s/2R$

### 3. The Improved CMS

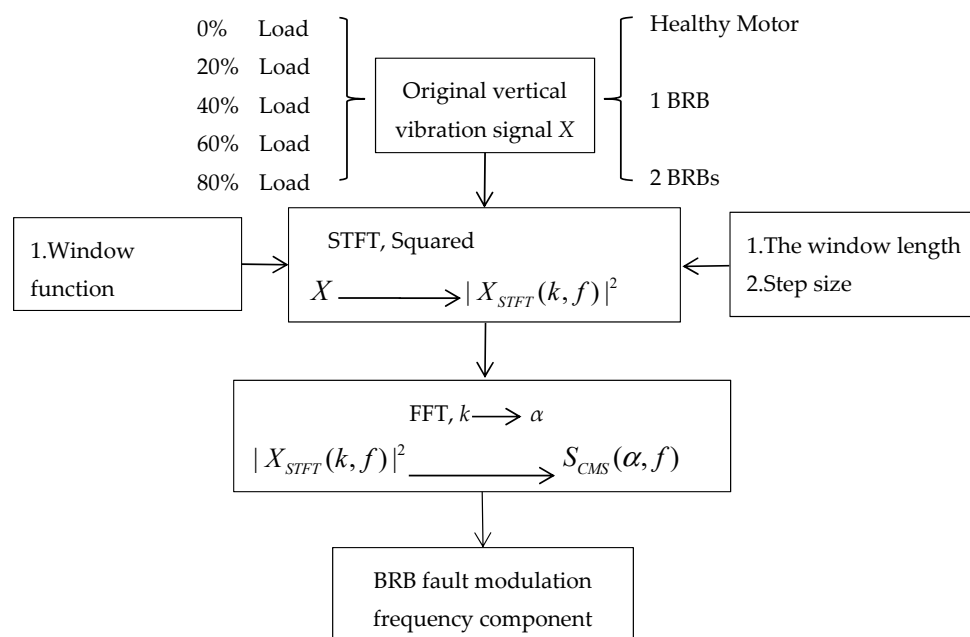
#### 3.1. The Window Function

The STFT is a powerful tool to process the non-stationary signal. It is applied by shifting a window function with a fixed window length and step size along the time axis of a signal, hence the signal can be divided into many segments in which it is regarded as a stationary signal [30]. The different window function has different performance parameters including the width of the main lobe, the peak of the minor lobe, and the rate of decay in the spectrum. The signals consisting of different fault forms must be processed with specific window functions as the appropriate window function is capable of improving the accuracy of fault identification. Otherwise, it is impossible to accurately extract the fault characteristics from the analyzed signals, so choosing the most suitable window function is an important step based on the fault that is being analyzed [31].

#### 3.2. The Window Length and Step Size

The window length and step size also play an important part in the STFT. The overlap between the two adjacent moving windows due to the appropriate step size can reduce the leakage of the spectrum. However, the different window length and step size can affect the computational efficiency of the STFT, which also increases the computational complexity of the CMS algorithm. Hence, it is necessary to select the appropriate window length and step size for a specific signal while guaranteeing the time resolution and frequency resolution [30].

In this regard, improved CMS method needs a two-step process in which the appropriate window function is chosen to enhance its sensitivity for identifying BRB faults, and then window length and step size are optimized in order to harvest a better computational benefit. A detailed flowchart of the proposed method is shown in Figure 1.

**Figure 1.** Flowchart of the proposed method.

#### 4. Simulation Study

In this section, a synthetic cyclostationary signal was established to validate the performance of the proposed method. The simulated signal is similar to the vibration signal obtained from the IMs with BRB faults at a steady-state operation. When the BRB fault occurs, the fault characteristic frequency of the rotor is a low frequency component, the rotation frequency of the rotating shaft is a high frequency component, and the low frequency related to the BRB fault is modulated on the rotating shaft frequency. The synthetic cyclostationary signal consists of a carrier frequency  $f_r$  showing the rotation frequency of rotation shaft, and a modulation frequency  $\alpha_0$  denoting the frequency component related to the BRB faults. The simulated signal  $x(t)$  consists of a carrier signal  $x_1(t)$ , a modulation signal  $x_2(t)$ , and a Gaussian white noise signal  $n(t)$  with a specific signal-to-noise ratio (SNR) of  $-2$  dB. The length of the samples  $L$  and sampling frequency  $F_s$  were  $10^6$  and 10 kHz, respectively. Where  $t = n/F_s$  ( $n = 0, 1, \dots, L - 1$ ) denotes the discrete time, and  $M_1, M_2$  represent the amplitude of a carrier signal and a modulation signal, respectively.  $M_1$  and  $M_2$  can indicate the energy of the carrier signal and the modulated signal and the different fault levels can be built by setting their values. In this study,  $M_1$  was set to 1, and  $M_2$  was set to 1 and 0.5 to represent 2 BRBs fault and 1 BRB fault cases. Moreover, the carrier frequency  $f_r$  was set to 40 Hz, and the modulation frequency  $\alpha_0$  was set to 4.27 Hz and 3.27 Hz to denote 2 BRBs fault and 1 BRB fault, respectively. Therefore, the simulation signals can be expressed as:

$$x(t) = (1 + M_2 \times x_2(t)) \times M_1 \times x_1(t) + n(t) \quad (8)$$

$$x_{1 \text{ BRB}}(t) = (1 + 0.5 \times \sin(2 \times \pi \times 3.27 \times t)) \times \sin(2 \times \pi \times 40 \times t) + n(t) \quad (9)$$

$$x_{2 \text{ BRBs}}(t) = (1 + \sin(2 \times \pi \times 4.27 \times t)) \times \sin(2 \times \pi \times 40 \times t) + n(t) \quad (10)$$

##### 4.1. The Improvement of Window Function

In order to determine the optimal window function, the different window functions were applied to the analysis with the same simulated data. The objective is to select the most suitable window function by analyzing the diagnosis results.

In this processing, the  $A_1$  and  $A_2$  respectively represent the amplitude of the characteristic frequencies  $\alpha_0$  of simulated 1 BRB and 2 BRBs faults. In addition,  $\eta$  is to show the failure level of 2 BRBs to 1 BRB. The higher the failure level is, the better of the selected window function can be in the classification of the BRB faults.

$$\eta = \frac{A_2 - A_1}{A_1} \times 100\% \quad (11)$$

As can be seen from Table 2, the flat top function is able to receive a higher BRB detection capability based on the simulated BRB fault signals. Obviously, its diagnostic power is more than four times that of the rectangular window function. As a result, the CMS method using the flat top function can get more accurate BRB diagnosis performance based on the simulated signals.

**Table 2.** The types of window function and their broken rotor bar (BRB) fault recognition capabilities in the simulation.

Window Fiction	$\eta$ (%)
Rectangular	6.95
Triangular	30.15
Blackman	28.37
Hanning	25.90
Bartlett	30.21
<b>Flat top</b>	<b>32.29</b>
Nuttal	30.23
Gaussian	28.03
Hamming	25.16
Kaiser ( $\beta = 1$ )	10.43
Kaiser ( $\beta = 2$ )	22.30
Kaiser ( $\beta = 3$ )	27.07
Kaiser ( $\beta = 4$ )	26.93
Kaiser ( $\beta = 5$ )	25.04

#### 4.2. The Improvement of the Window Length and Step Size

To get a better computational gain of the CMS algorithm, the flat top function with the window length of  $2^6$ ,  $2^7$ ,  $2^8$ , and  $2^9$  was respectively used in the simulation. Additionally, the step size was selected as 25%, 30%, 35%, 40%, 45%, and 50% of the flat top window length, respectively, which ensures that the overlap between two adjacent moving windows is between 50% and 75% to reduce spectrum leakage and the effect of window length and step size on BRB fault identification. The step size was selected to be an integer according to the rounding principle. For example, if the window length is  $2^6$ , then the step size is chosen as follows: 16, 19, 22, 26, 29, and 32. The simulated results are shown in Figure 2.

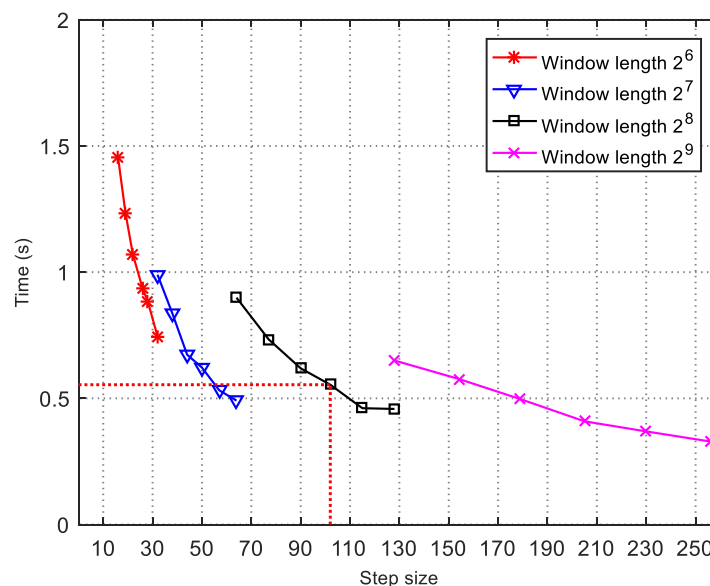


**Figure 2.** Simulated time required for different step sizes in four window lengths.

Thus, in order to ensure time efficiency, the window length of  $2^8$  and the step size of 40% of the window length were selected for the CMS operation. The appropriate step size used for the simulation study was 102 and the required simulation time was only 0.554 s as shown in Figure 2. All simulations and their experimental data processing were performed on a computer with a i5-7400 CPU processor 3.00 GHz. The parameter values used in the improved CMS algorithm and calculation time for all

algorithms utilized in synthetic simulation are presented in Table 3. The improved CMS not only ensures the optimal BRB fault identification accuracy based on the existing window functions, but also improves the calculation efficiency.

**Table 3.** Simulated parameters and calculation time used in the five algorithms.

Parameters and Methods	Setting and Time
Window	Flat top
$Nw$	$2^8$
$R$	102
$\Delta\alpha$	0.01 Hz
PSD	0.0630 s
CPS	185.7380 s
ACP	$7.0652 \times 10^3$ s
Improved CMS	0.5540 s
FSC	1.6160 s

The optimized window length and step size make only 0.5540 s is taken by the improved CMS method, in which its computational efficiency is only second to conventional PSD method as shown in Table 3. In the synthetic simulation, the characteristic frequency can be clearly extracted by several algorithms and the order of computational efficiency is PSD > CMS > FSC > CPS > ACP. However, it is worth mentioning that the simulation time of the ACP algorithm takes approximately  $7.0652 \times 10^3$  s, which is far from the computational efficiency of other algorithms. This is the reason why this algorithm is greatly limited in practical applications. Considering the higher computational cost and lower value of the ACP algorithm in practical applications, in the following study, ACP will not be applied to the processing of the experimental data.

According to the simulation Equation (10), the improved CMS algorithm with the flat top window function can extract the fault characteristic frequency from the simulated signals with a SNR of  $-30$  dB as shown in Figure 3. This offers an excellent immunity to noise in the measurements. Therefore, the CMS method can be improved to give optimal analysis results based on the flat top function, with a window length of  $2^8$ , and step size of 40% of the window length.

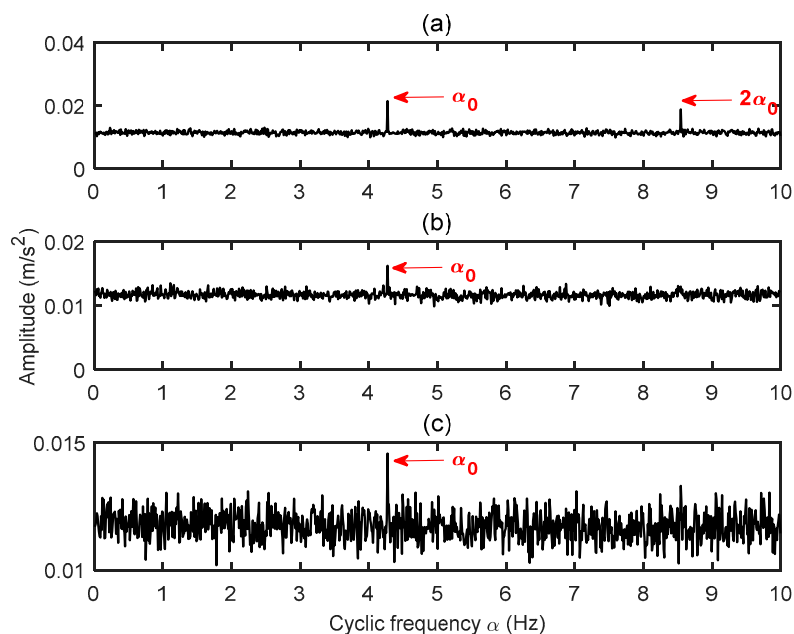


**Figure 3.** The analysis results for simulated signals using the improved cyclic modulation spectrum (CMS) with (a) signal-to-noise ratio (SNR) = 0 dB, (b) SNR =  $-18$  dB, and (c) SNR =  $-30$  dB.

## 5. Experimental Verification

### 5.1. Experiment Setup

To prove the efficiency and performance of the proposed approach in the BRB fault diagnosis, a special IM test platform was employed to acquire vibration data from three IMs with the same specification, with a baseline and two different degrees of BRB severity motors. Figure 4 illustrates the main structure of the experimental setup used in this study. The experimental system consists of a DC load generator, a flexible coupling, an AC drive motor, an encoder, a thermocouple, a horizontal accelerometer, and a vertical accelerometer. The AC drive motor is a 2-pole pairs, 3-phase motor and the supply fundamental frequency and synchronous speed are 50 Hz and 1500 rpm, respectively. In the meantime, the two different BRB fault cases are shown in Figure 5. As illustrated in Figure 5a,b, the BRB fault conditions are complete bar breakages that have been artificially produced by completely drilling one bar to its full depth. These motors will eventually be tested under different loads to evaluate the performance of the improved CMS method.

Moreover, to estimate the influence of the operating conditions on the fault detection performance, the vertical vibration signals were measured under a series of loads from 0%, 20%, 40%, 60 to 80% of the full working load at the rated speed. All test signals were simultaneously measured using a multi-channel data acquisition system with a sampling frequency of 96 kHz. A data length of 30 s was acquired for each working condition to guarantee the integrity and accuracy of the information. In this study, the improved CMS method is validated based on the optimization of the window function, window length, and step size.

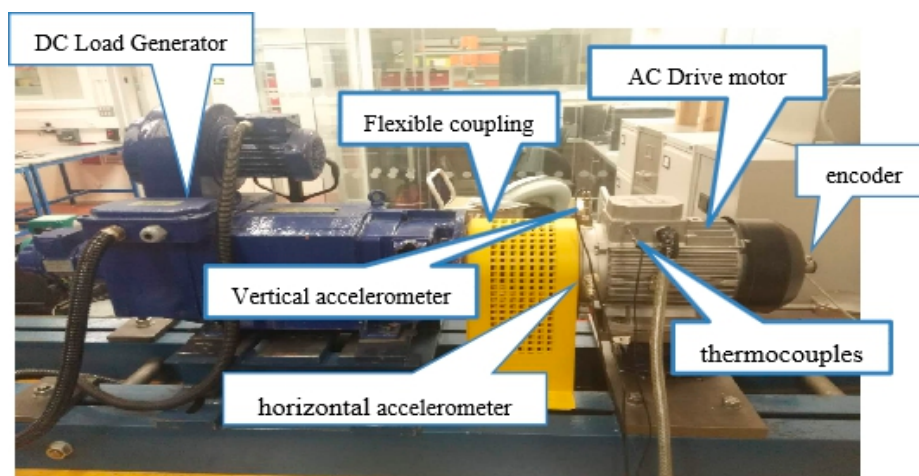


Figure 4. Experimental platform of the induction motor system.



Figure 5. The different induction motors with (a) 1 BRB, and (b) 2 BRBs fault.

## 5.2. Parameter Optimization for CMS Application

### 5.2.1. The Selection of Window Function

The different window functions were applied to the analysis of the same experimental data to select the optimal window function. The objective is to select the most suitable window function for obtaining accurate diagnosis results, which not only can obtain the best accuracy for identifying the BRB fault types and severities, but also can basically reflect the law that the amplitude of the characteristic frequency related to BRB faults increases with increasing the loads.

In this paper, the  $A_{0,k}$ ,  $A_{1,k}$ , and  $A_{2,k}$  ( $k = 1, 2, 3, 4, 5$ ) respectively represents the sum of the amplitudes of the characteristic frequencies  $2sf_0$  of healthy motor, and the faulty motors with 1 BRB and 2 BRBs under five different loads. In addition,  $\eta_{1 BRB}$ ,  $\eta_{2 BRB}$ , and  $\eta_{2-1 BRB}$  indicate the failure level of 1 BRB, 2 BRBs, and the fault level of 2 BRBs with respect to 1 BRB as follows:

$$\begin{aligned}\eta_{1 BRB} &= \frac{A_{1,k} - A_{0,k}}{A_{0,k}} \times 100\% \\ \eta_{2 BRB} &= \frac{A_{2,k} - A_{0,k}}{A_{0,k}} \times 100\% \\ \eta_{2-1 BRB} &= \frac{A_{2,k} - A_{1,k}}{A_{1,k}} \times 100\%\end{aligned}\quad (12)$$

Through the analysis, it can be found that only the rectangular window and some Kaiser windows with some  $\beta$  parameters cannot show the trend that the amplitude of the characteristic frequency  $2sf_0$  increases with increasing the loads. However, the other window functions presented in Table 4 can reflect this feature, and different window functions still have different identification abilities of BRB fault types and severities.

**Table 4.** The types of window function and their BRB fault identification capabilities in the experiments.

Window Fiction	$\eta_{1 BRB}$ (%)	$\eta_{2 BRB}$ (%)	$\eta_{2-1 BRB}$ (%)
Triangular	197.71	359.60	54.37
Blackman	198.81	356.05	52.62
Hanning	203.69	358.54	50.98
Bartlett	221.38	400.53	55.74
Flat top	296.73	480.62	46.35
Nuttal	231.94	469.87	71.68
Gaussian	244.28	489.09	71.85
Hamming	246.71	494.29	71.41
<b>Kaiser (<math>\beta = 3</math>)</b>	<b>262.05</b>	<b>527.32</b>	<b>73.27</b>
Kaiser ( $\beta = 3.5$ )	255.08	508.41	71.20
Kaiser ( $\beta = 4$ )	250.79	499.20	70.86
Kaiser ( $\beta = 5$ )	245.95	488.66	70.16

From the analysis results presented in Table 4,  $\eta_{1 BRB}$ ,  $\eta_{2 BRB}$ , and  $\eta_{2-1 BRB}$  have larger values in the Kaiser ( $\beta = 3$ ) window function than other window functions because the parameter  $\beta$  can effectively adjust the relative proportion of the width of the main lobe and the rate of decay in the spectrum. This indicates this window function has higher identification capabilities of BRB fault types and severities. Hence, the Kaiser ( $\beta = 3$ ) window was selected as the window function executed by the CMS.

### 5.2.2. The Selection of Window Length and Step Size

In the next step, the Kaiser ( $\beta = 3$ ) window function with the window length of  $2^6$ ,  $2^7$ ,  $2^8$ , and  $2^9$  was respectively used in the experimental analysis and the step size was still selected as 25%, 30%, 35%, 40%, 45%, and 50% of Kaiser ( $\beta = 3$ ) window length.

All the experimental consumption of several step sizes in the four window lengths are illustrated in Figure 6. The window length of  $2^8$  and the step size of 40% of the window length were eventually selected for guaranteeing the accuracy and time efficiency of the CMS algorithm in BRB fault detection. Moreover, the calculation time was 26.1710 s. Finally, the improved CMS with the Kaiser ( $\beta = 3$ ) function, the window length of  $2^8$ , and the step size of 40% of the window length was applied to the experimental validation. According to Table 1, the cyclic frequency resolution  $\Delta\alpha$  was approximately 0.03 Hz and the maximum cycle frequency  $\alpha_{max}$  for improved CMS analysis was 375 Hz according to the selected window length. This considerably satisfies the extraction of the BRB fault characteristics because the modulation information causing the BRB faults is a low frequency component.

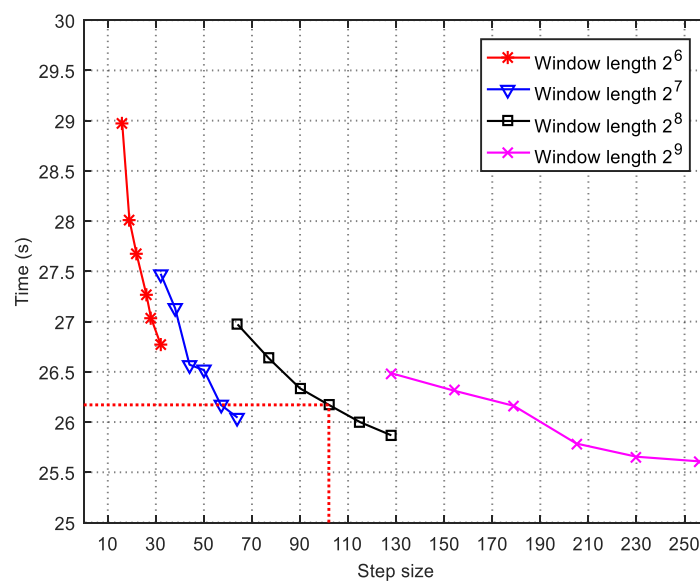


**Figure 6.** The experimental time required for different step sizes in the four window lengths.

### 5.3. Experimental Results

As mentioned above, the characteristic frequency  $\alpha_0 = 2sf_0$  ( $f_0 = 50$  Hz) is known to be the most obvious component related to BRB faults. Table 5 illustrates the slips of IMs with different fault cases under different load conditions. The detection results obtained by the analysis of the PSD, CPS, FSC, and the improved CMS method respectively are shown in Figures 7–10.

**Table 5.** The slips and characteristic frequencies of three fault cases under different loads.

Load	Slip (s)			Characteristic Frequency $\alpha_0 = 2sf_0$ (Hz)
	Healthy Motor	1 BRB	2 BRBs	
0%	0.0012	0.0020	0.0020	0.12/0.20/0.20
20%	0.0080	0.0092	0.0097	0.80/0.92/0.97
40%	0.0148	0.0172	0.0180	1.48/1.72/1.80
60%	0.0228	0.0268	0.0270	2.28/2.68/2.70
80%	0.0308	0.0372	0.0400	3.08/3.72/4.00

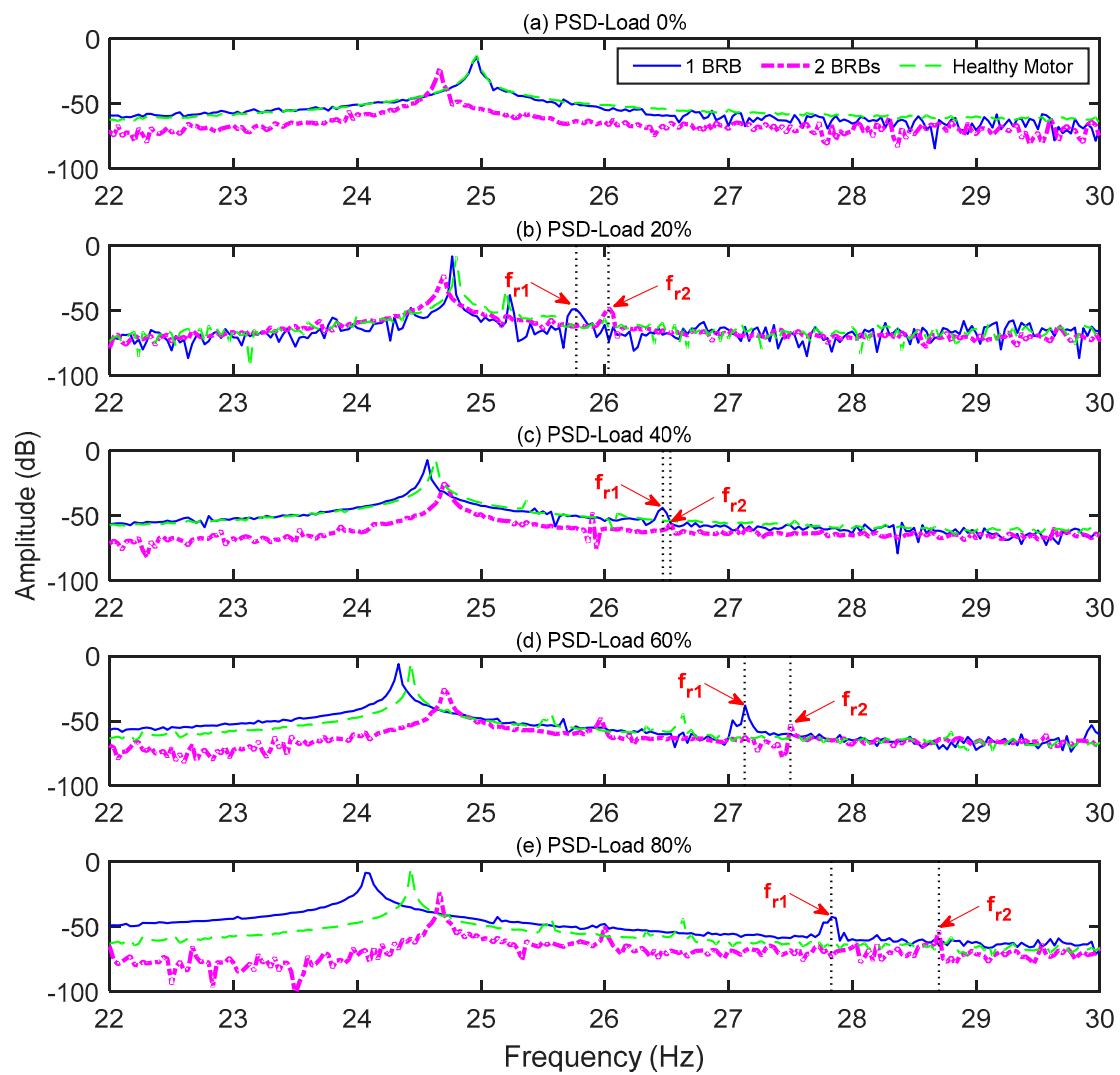


**Figure 7.** The right sideband components  $f_{r1}$  and  $f_{r2}$  for 1 BRB and 2 BRBs based on the power spectral density (PSD) method at (a) 0% load, (b) 20% load, (c) 40% load, (d) 60% load, and (e) 80% load under operating conditions. Blue for 1 BRB, Pink for 2 BRBs, and Green under healthy motor.

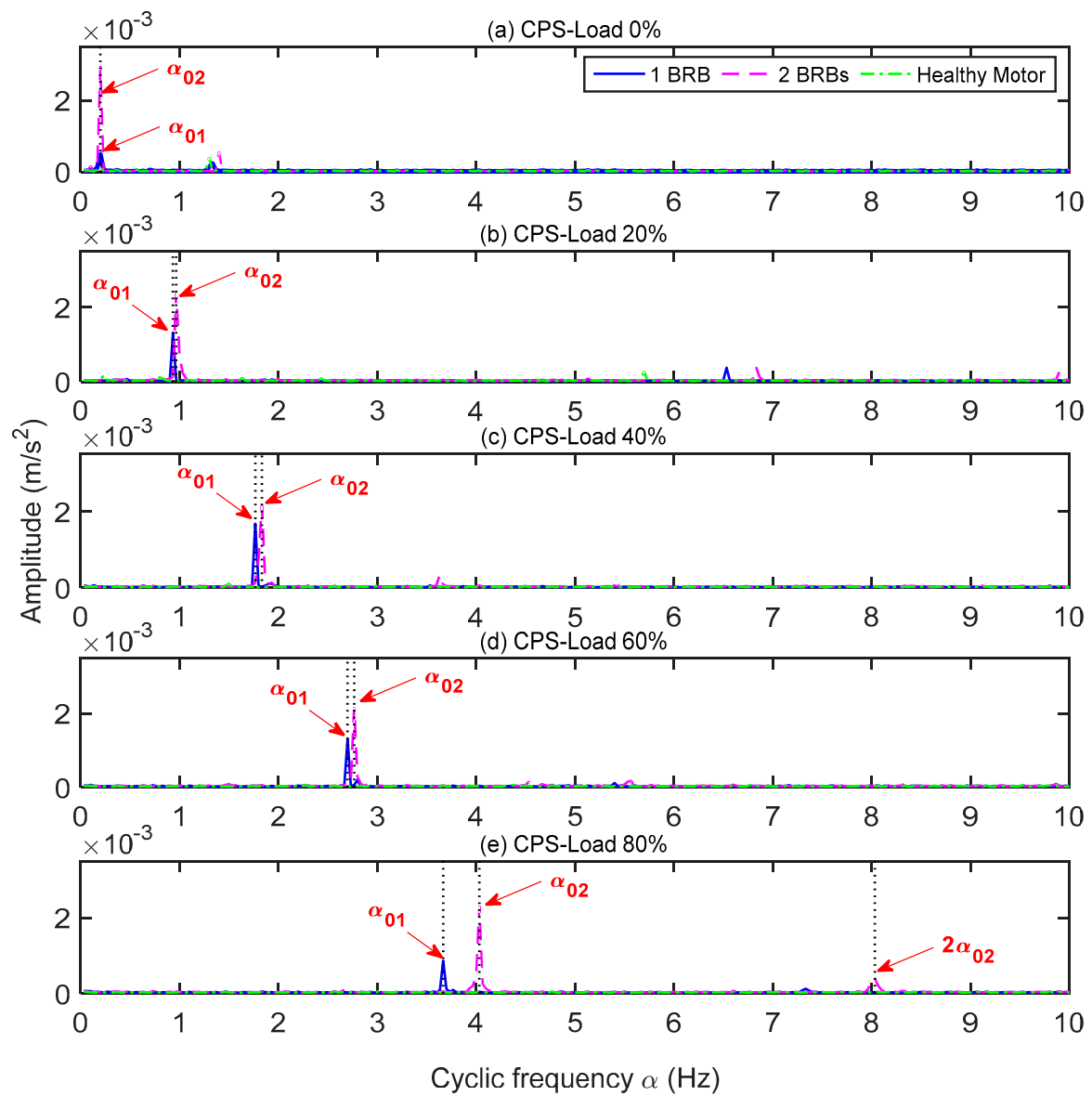


**Figure 8.** The characteristic frequencies of  $\alpha_{01}$  and  $\alpha_{02}$  for 1 BRB and 2 BRBs based on the cyclic power spectrum (CPS) method at (a) 0% load, (b) 20% load, (c) 40% load, (d) 60% load, and (e) 80% load under operating condition. Blue for 1 BRB, Pink for 2 BRBs, and Green under healthy motor.

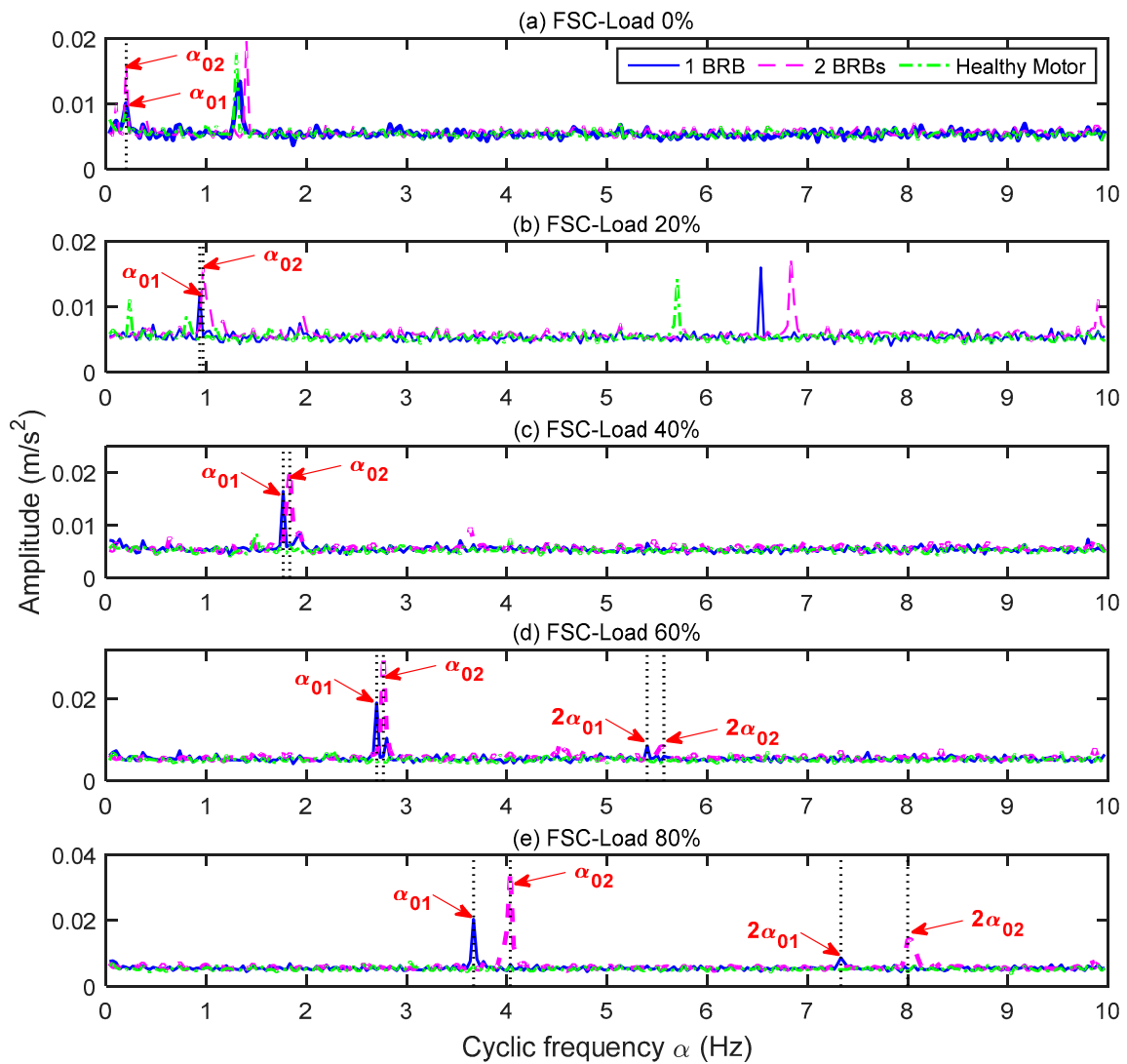


**Figure 9.** The characteristic frequencies of  $\alpha_{01}$  and  $\alpha_{02}$  for 1 BRB and 2 BRBs based on FSC method at (a) 0% load, (b) 20% load, (c) 40% load, (d) 60% load, and (e) 80% load under operating condition. Blue for 1 BRB, Pink for 2 BRBs, and Green under healthy motor.

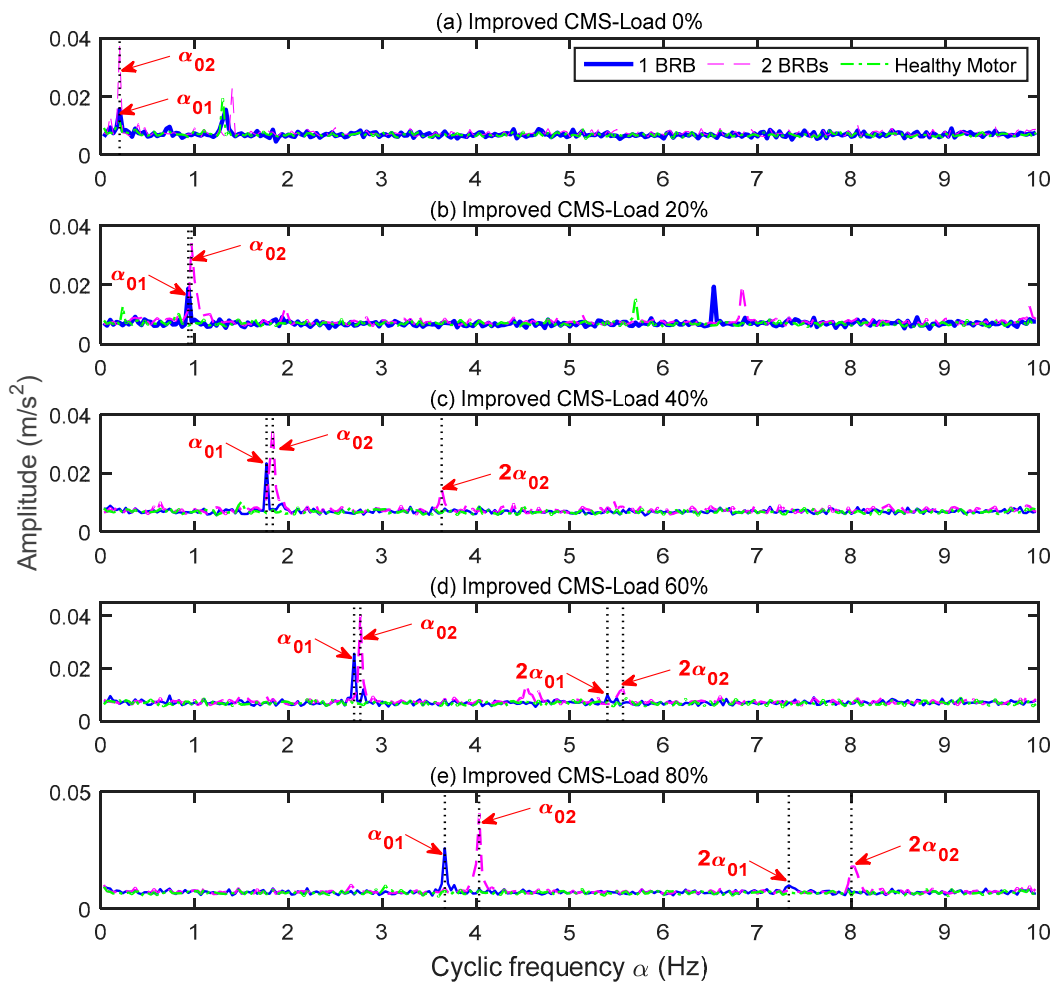


**Figure 10.** The characteristic frequencies of  $\alpha_{01}$  and  $\alpha_{02}$  for 1 BRB and 2 BRBs based on the improved CMS method at (a) 0% load, (b) 20% load, (c) 40% load, (d) 60% load, and (e) 80% load under operating conditions. Blue for 1 BRB, Pink for 2 BRBs, and Green under healthy motor.

#### 5.4. Results Discussion

As observed in Figure 7, the characteristic frequency components related to BRB faults obtained by PSD are weak, especially in light loads. Further, only the right sidebands can present BRB fault peaks clearly. Table 6 shows the characteristic frequency components obtained by the four methods under different load conditions for two BRB faults detection. Compared to the theoretical characteristic frequency components presented in Table 5, it can be seen the PSD method can only roughly reflect the fault information and it cannot present any fault symptoms when the load is 0%. Hence, regarding the non-linear and non-stationary vibration signals produced by BRB faults, the PSD approach fails to extract BRB fault information accurately, especially for vibration signals with high noise.

By contrast, the cyclic spectral analysis methods indeed provide a better analysis for processing non-stationary signals since the signals are processed based on the cyclostationary level. According to the results from cyclic spectral analysis as shown in Figures 8–10, the three algorithms can obviously exhibit BRB fault features better than conventional PSD methods. In addition, the three cyclic spectral analysis methods are able to accurately extract characteristic frequencies about BRB faults according to the results as shown in Tables 5 and 6, while three approaches have different discrimination capabilities of BRB fault types and severities.

**Table 6.** The different characteristic frequencies detected by four methods under different loads.

Load	PSD (Hz)		CPS (Hz)		FSC (Hz)		Improved CMS (Hz)	
	1 BRB	2 BRBs	1 BRB	2 BRBs	1 BRB	2 BRBs	1 BRB	2 BRBs
0%	-	-	0.200	0.200	0.200	0.200	0.200	0.200
20%	1.333	1.000	0.933	0.967	0.933	0.967	0.933	0.967
40%	1.830	1.900	1.767	1.833	1.767	1.833	1.767	1.833
60%	2.800	2.800	2.700	2.767	2.700	2.767	2.700	2.767
80%	3.770	4.030	3.667	4.033	3.667	4.033	3.667	4.033

Furthermore, the amplitude of the fault characteristic frequency can be applied to distinguish the fault types, and theoretically, the amplitude will be increased along with the increasing of fault severities. Typically, the BRB fault severity will also be increased along with the increasing of operating loads for all the BRB fault case. Firstly, as can be observed in Figure 11a, the fault information obtained by PSD cannot obviously provide clear distinctions for the different BRB fault types and severities under different operating loads. Secondly, although the CPS method can reflect the BRB fault types as shown in Figure 11b, this method cannot accurately show that the BRB fault severity increases with increasing the loads. In contrast, the FSC method has the advantage of reflecting the trend and distinguishing the BRB fault types as shown in Figure 11c, but this method has a lower accuracy for the detection of BRB fault types under various operating conditions, which is not conducive to the diagnosis and discrimination of BRB fault types.

For comparison purposes, the CMS algorithm with the same window length and step size as the improved CMS method but with Hanning window function was applied to the experimental analysis. According to the diagnostic results as shown in Figure 11d, while the CMS method spends the same amount of time in processing the same data, it presents a lower diagnostic accuracy for BRB faults. Similarly, Figure 11e shows the result analyzed by the CMS method with the Kaiser ( $\beta = 3$ ) window, but with the window length of  $2^7$  and the step size of 30% of the window length. The diagnosis results obtained by the improved CMS method with the Kaiser ( $\beta = 3$ ) window, the window length of  $2^8$ , and the step size of 40% of the window length is shown in Figure 11f. This CMS method with different window lengths and step sizes has similar accuracy to the BRB faults detection. However, 27.1340 s are consumed by this CMS as illustrated in Figure 6 compared to 26.1710 s taken by the improved CMS method.

Moreover, based on the analysis results presented in Figure 11f, the improved CMS can exhibit larger distinctions between a healthy motor, and a faulty motor with 1 BRB and 2 BRBs. The improved CMS algorithm with the Kaiser ( $\beta = 3$ ) window can provide a higher sensitivity for BRB faults diagnosis than other methods presented in Figure 11, which is due to the parameter optimization for the CMS applications.

Most importantly, the improved CMS algorithm significantly minimizes the computational costs, and approximately 26.1710 s as shown in Table 7 is utilized to obtain better diagnosis results than the other two algorithms owing to the optimization of the window length and the step size. However, the CPS approach consumes substantial computational time, which takes approximately  $2.4028 \times 10^4$  s to process and analyze the data containing 2,880,000 sampling points. Therefore, the improved CMS algorithm is indeed an efficient cyclic spectral analysis algorithm to analyze and detect the BRB faults in IMs.

**Table 7.** Computing consumption of the three algorithms in experimental processing.

	CPS	FSC	Improved CMS
Time (s)	$2.4028 \times 10^4$	30.2250	26.1710

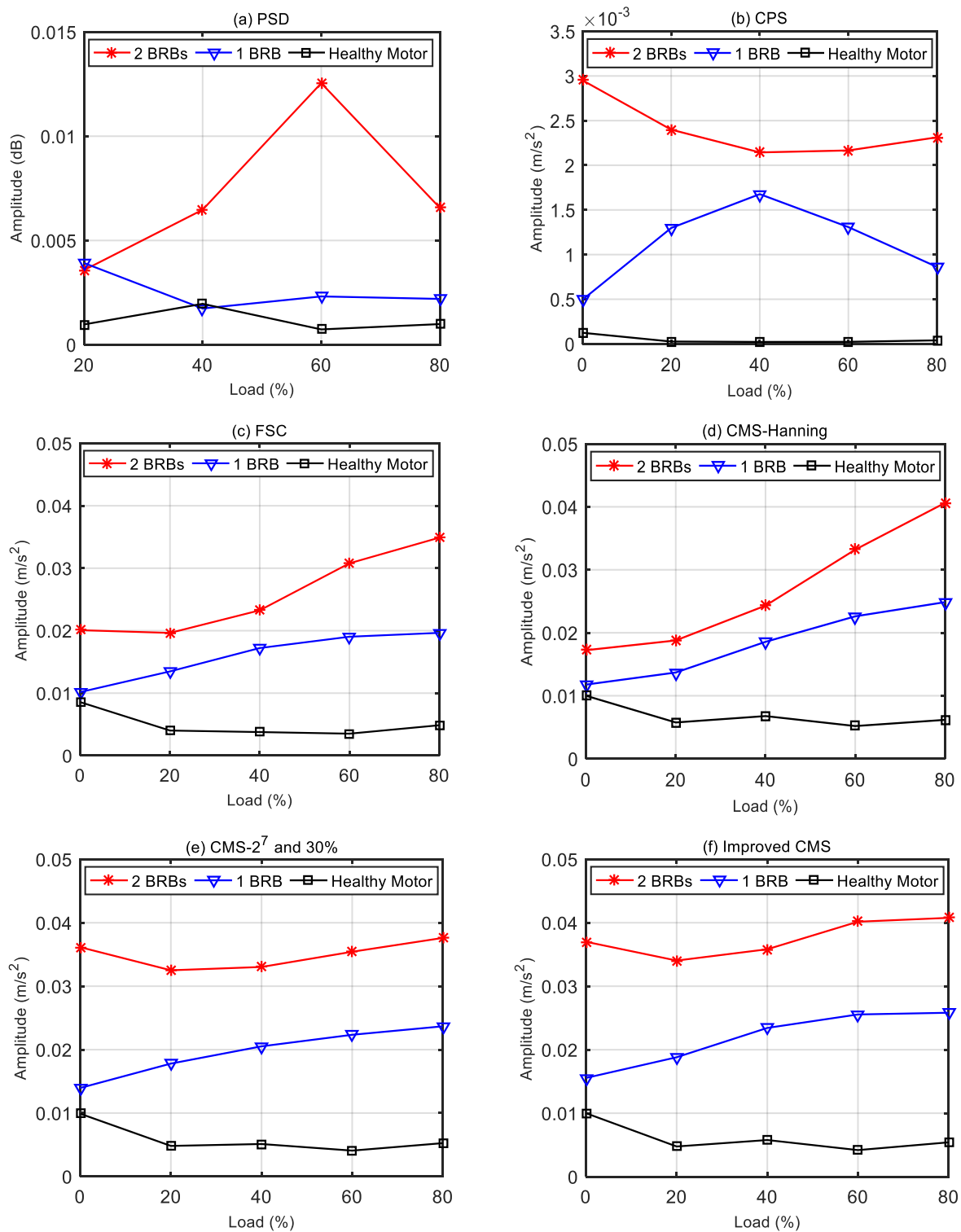


**Figure 11.** The amplitudes of characteristic frequency component  $\alpha_0$  under different loads in three BRB cases extracted by (a) PSD, (b) CPS, (c) fast spectral correlation (FSC), (d) CMS with Hanning window function, (e) CMS with window length of  $2^7$  and step size of 30% of the window length, and (f) the improved CMS, respectively.

## 6. Conclusions

In this paper, an improved CMS fault feature extraction method based on the optimization of a window function, length and step size for the STFT was proposed for BRB fault diagnosis. The efficiency

and performance of the proposed method was validated based on the simulation and experimental studies. Both the simulation and experimental studies presented that the window function having more influence on the accuracy of BRB fault diagnosis and the window length and step size can affect the efficiency of the CMS method. In simulation studies, the synthetic signals with different SNRs are simulated and analyzed. The analysis results show the proposed method has high noise immunity and is able to accurately extract BRB fault features. The computational efficiency of the improved CMS is not only optimized but also outperformed other cyclostationary analysis methods based on the comparison analysis. The experimental study validated the ability of the improved CMS method for diagnosing and classifying healthy motors, and faulty motors with 1 BRB and 2 BRBs under different operating conditions with higher accuracy and lower computational costs. It demonstrated that the improved CMS method gives more sensitivity than other cyclic spectral analysis estimators for BRB failures detection. Therefore, the improved CMS approach can be considered as a promising online fault diagnostic technique with higher sensitivity, and its applicability for online fault diagnosis of various machines could receive further consideration due to its robustness and efficiency.

**Author Contributions:** Conceptualization, J.Y., D.Z. and F.G.; formal analysis, Z.W.; funding acquisition, D.Z.; investigation, H.L. and Y.X.; Methodology, J.Y., D.Z. and F.G.; project administration, D.Z.; resources, D.Z. and F.G.; Software, Z.W.; writing—Original draft, Z.W.; writing—Review and editing, J.Y., D.Z., H.L., Y.X. and F.G.

**Funding:** This research was funded by the Hebei Provincial International Science and Technology Cooperation Program of China, grant number 17394303D and the National Natural Science Foundation of China, grant number 51605133, 51705127.

**Acknowledgments:** The authors would like to thank Centre for Efficiency and Performance Engineering (CEPE) at the University of Huddersfield for providing the materials used for experiments. Meanwhile, the authors would like to thank the anonymous reviewers and the editor for their valuable comments and suggestions.

**Conflicts of Interest:** The authors declare no conflict of interest.

## References

1. Choudhary, A.; Goyal, D.; Shimi, S.L.; Akula, A. Condition Monitoring and Fault Diagnosis of Induction Motors: A Review. *Arch. Comput. Methods Eng.* **2018**, *25*, 1–18. [[CrossRef](#)]
2. Gritli, Y.; Di Tommaso, A.O.; Filippetti, F.; Miceli, R.; Rossi, C.; Chatti, A. Investigation of motor current signature and vibration analysis for diagnosing rotor broken bars in double cage induction motors. In Proceedings of the International Symposium on Power Electronics Power Electronics, Electrical Drives, Automation and Motion, Sorrento, Italy, 20–22 June 2012; IEEE: Piscataway, NJ, USA, 2012; pp. 1360–1365.
3. Martinez, J.; Belahcen, A.; Muetze, A. Analysis of the vibration magnitude of an induction motor with different numbers of broken bars. *IEEE Trans. Ind. Appl.* **2017**, *53*, 2711–2720. [[CrossRef](#)]
4. Shakya, P.; Kulkarni, M.S.; Darpe, A.K. Bearing diagnosis based on Mahalanobis–Taguchi–Gram–Schmidt method. *J. Sound Vib.* **2015**, *337*, 342–362. [[CrossRef](#)]
5. Gritli, Y.; Di Tommaso, A.O.; Miceli, R.; Filippetti, F.; Rossi, C. Vibration signature analysis for rotor broken bar diagnosis in double cage induction motor drives. In Proceedings of the 4th International Conference on Power Engineering, Energy and Electrical Drives, Istanbul, Turkey, 13–17 May 2013; IEEE: Piscataway, NJ, USA, 2013; pp. 1814–1820.
6. Climente-Alarcon, V.; Antonino-Daviu, J.A.; Vedreno-Santos, F.; Puche-Panadero, R. Vibration Transient Detection of Broken Rotor Bars by PSH Sidebands. *IEEE Trans. Ind. Appl.* **2013**, *49*, 2576–2582. [[CrossRef](#)]
7. Rangel-Magdaleno, J.; Peregrina-Barreto, H.; Ramirez-Cortes, J.; Morales-Caporal, R.; Cruz-Vega, I. Vibration Analysis of Partially Damaged Rotor Bar in Induction Motor under Different Load Condition Using DWT. *Shock. Vib.* **2016**, *2016*, 1–11. [[CrossRef](#)]
8. Delgado-Arredondo, P.A.; Morinigo-Sotelo, D.; Osornio-Rios, R.A.; Avina-Cervantes, J.G.; Rostro-Gonzalez, H.; Romero-Troncoso, R.D.J. Methodology for fault detection in induction motors via sound and vibration signals. *Mech. Syst. Signal. Process.* **2017**, *83*, 568–589. [[CrossRef](#)]
9. Morales-Perez, C.; Rangel-Magdaleno, J.; Peregrina-Barreto, H.; Amezcua-Sanchez, J.P.; Valtierra-Rodriguez, M. Incipient Broken Rotor Bar Detection in Induction Motors Using Vibration Signals and the Orthogonal Matching Pursuit Algorithm. *IEEE Trans. Instrum. Meas.* **2018**, *67*, 2058–2068. [[CrossRef](#)]

10. Camarena-Martinez, D.; Valtierra-Rodriguez, M.; Garcia-Perez, A.; Osornio-Rios, R.A.; Romero-Troncoso, R.D.J. Empirical Mode Decomposition and Neural Networks on FPGA for Fault Diagnosis in Induction Motors. *Sci. World J.* **2014**, *2014*, 1–17. [[CrossRef](#)]
11. Rangel-Magdaleno, J.; Peregrina-Barreto, H.; Ramirez-Cortes, J.; Cruz-Vega, I. Hilbert spectrum analysis of induction motors for the detection of incipient broken rotor bars. *Measurement* **2017**, *109*, 247–255. [[CrossRef](#)]
12. Morinigo-Sotelo, D.; Romero-Troncoso, R.D.J.; Panagiotou, P.A.; Antonino-Daviu, J.A.; Gyftakis, K.N. Reliable detection of rotor bars breakage in induction motors via MUSIC and ZSC. *IEEE Trans. Ind. Appl.* **2017**, *54*, 1224–1234. [[CrossRef](#)]
13. Camarena-Martinez, D.; Perez-Ramirez, C.A.; Valtierra-Rodriguez, M.; Amezcua-Sanchez, J.P.; Romero-Troncoso, R. Synchrosqueezing transform-based methodology for broken rotor bars detection in induction motors. *Measurement* **2016**, *90*, 519–525. [[CrossRef](#)]
14. Ceban, A.; Pusca, R.; Romary, R. Study of rotor faults in induction motors using external magnetic field analysis. *IEEE Trans. Electron.* **2011**, *59*, 2082–2093. [[CrossRef](#)]
15. Picazo-Ródenas, M.; Antonino-Daviu, J.A.; Climente-Alarcon, V.; Royo-Pastor, R.; Mota-Villar, A. Combination of non-invasive approaches for general assessment of induction motors. In Proceedings of the 2014 International Conference on Electrical Machines (ICEM), Berlin, Germany, 2–5 September 2014; IEEE: Piscataway, NJ, USA, 2014; pp. 1496–1502.
16. da Silva, A.M.; Povinelli, R.J.; Demerdash, N.A. Rotor Bar Fault Monitoring Method Based on Analysis of Air-Gap Torques of Induction Motors. *IEEE Trans. Ind. Inform.* **2013**, *9*, 2274–2283. [[CrossRef](#)]
17. Antoni, J. Cyclostationarity by examples. *Mech. Syst. Signal Process.* **2009**, *23*, 987–1036. [[CrossRef](#)]
18. Gardner, W. Exploitation of spectral redundancy in cyclostationary signals. *IEEE Signal. Process. Mag.* **1991**, *8*, 14–36. [[CrossRef](#)]
19. Borghesani, P. The envelope-based cyclic periodogram. *Mech. Syst. Signal. Process.* **2015**, *58*, 245–270. [[CrossRef](#)]
20. Antoni, J.; Hanson, D. Detection of Surface Ships from Interception of Cyclostationary Signature with the Cyclic Modulation Coherence. *IEEE J. Ocean. Eng.* **2012**, *37*, 478–493. [[CrossRef](#)]
21. Gu, F.; Shao, Y.; Hu, N.; Naid, A.; Ball, A.; Ball, A. Electrical motor current signal analysis using a modified bispectrum for fault diagnosis of downstream mechanical equipment. *Mech. Syst. Signal. Process.* **2011**, *25*, 360–372. [[CrossRef](#)]
22. Oviedo, S.J.; Quiroga, J.; Borrás, C. Experimental evaluation of motor current signature and vibration analysis for rotor broken bars detection in an induction motor. In Proceedings of the 2011 International Conference on Power Engineering, Energy and Electrical Drives, Malaga, Spain, 11–13 May 2011; IEEE: Piscataway, NJ, USA, 2011; pp. 1–6.
23. Bellini, A.; Concari, C.; Franceschini, G.; Tassoni, C.; Toscani, A. Vibrations, currents and stray flux signals to assess induction motors rotor conditions. In Proceedings of the IECON 2006—32nd Annual Conference on IEEE Industrial Electronics, Paris, France, 6–10 November 2006; IEEE: Piscataway, NJ, USA, 2006; pp. 4963–4968.
24. Rangel-Magdaleno, J.; Romero-Troncoso, R.; Osornio-Rios, R.; Cabal-Yepez, E.; Contreras-Medina, L. Novel Methodology for Online Half-Broken-Bar Detection on Induction Motors. *IEEE Trans. Instrum. Meas.* **2009**, *58*, 1690–1698. [[CrossRef](#)]
25. Kumar, T.C.A.; Singh, G.; Naikan, V.N.A. Effectiveness of vibration and current monitoring in detecting broken rotor bar and bearing faults in an induction motor. In Proceedings of the 2016 IEEE 6th International Conference on Power Systems (ICPS), New Delhi, India, 4–6 March 2016; IEEE: Piscataway, NJ, USA, 2016; pp. 1–5.
26. Antoni, J. Cyclic spectral analysis in practice. *Mech. Syst. Signal. Process.* **2007**, *21*, 597–630. [[CrossRef](#)]
27. Boustany, R.; Antoni, J. Cyclic spectral analysis from the averaged cyclic periodogram. *IFAC Proc. Vol.* **2005**, *38*, 166–171. [[CrossRef](#)]
28. Antoni, J.; Xin, G.; Hamzaoui, N. Fast computation of the spectral correlation. *Mech. Syst. Signal. Process.* **2017**, *92*, 248–277. [[CrossRef](#)]
29. Singh, G.; Naikan, V. Detection of half broken rotor bar fault in VFD driven induction motor drive using motor square current MUSIC analysis. *Mech. Syst. Signal. Process.* **2018**, *110*, 333–348. [[CrossRef](#)]

30. Brito, N.S.D.; de Souza, B.A.; dos Santos, W.C.; de Andrade Fortunato, L.M. Analysis of the influence of the window used in the Short-Time Fourier Transform for High Impedance Fault detection. In Proceedings of the 2016 17th International Conference on Harmonics and Quality of Power (ICHQP), Belo Horizonte, Brazil, 16–19 October 2016; IEEE: Piscataway, NJ, USA, 2016; pp. 350–355.
31. Yuegang, W.; Shao, J.; Hongtao, X. Non-stationary Signals Processing Based on STFT. In Proceedings of the 2007 8th International Conference on Electronic Measurement and Instruments, Xi'an, China, 16–18 August 2007; IEEE: Piscataway, NJ, USA, 2007.



© 2019 by the authors. Licensee MDPI, Basel, Switzerland. This article is an open access article distributed under the terms and conditions of the Creative Commons Attribution (CC BY) license (<http://creativecommons.org/licenses/by/4.0/>).